Preprints of the 21st IFAC World Congress (Virtual)
Berlin, Germany, July 12-17, 2020

Finite Element Simulation Based Analysis of Valve-sparing Aortic Root Surgery

Róbert Nagy * **Tamás Umenhoffer** * **Péter Somogyi** *
Ákos Szlávecz * **Anikó Kubovje** * **Bernhard Laufer** ***
Katalin Kovács **** **Tamás Szerafin** ** **Balázs Benyó** *

* *Budapest University of Technology and Economics, Budapest, Hungary.*
** *University of Debrecen, Debrecen, Hungary*
*** *Furtwangen University, Villingen-Schwenningen, Germany*
**** *Széchenyi István University, Győr, Hungary*

Abstract: The valve-sparing aortic root surgery is frequently used in the treatment of aortic root enlargement or aortic root aneurysm. The currently used common surgical practice assumes that the valve leaflets are distributed evenly around the circle defined by the aorta wall which is frequently a false assumption according to hart anatomy studies. A finite element simulation based method is proposed in this study for the analysis of the alternative surgical outcomes of the valve-sparing aortic root surgery. The simulation methods allow the definition of the aortic valve leaflet commissure positions and the diameter of the graft used to replace the aortic root. The suggested methods are able to estimate and quantitatively compare the hemodynamic functions and the robustness of the aortic valve functions. The corresponding modeling environment makes possible the easy definition of the patient specific aortic root model that is used as an input of the simulation. The initial validation of the simulation method was done by a real patient data based simulation study. These results suggest that the currently used surgical practice can be improved.

Keywords: modeling and simulation, geometric aortic valve model, elastic and fluid simulation

1. INTRODUCTION

The most common diseases causing aortic root enlargement or aortic root aneurysm (Teo and Isselbacher) are the high blood pressure and Marfan syndrome. Unlike in case of aortic valve stenosis, when the calcification makes the valves stiff and narrow, in the case of these diseases the aortic valve is not affected. Thus the so-called David procedure (David (2010)), the valve-sparing aortic root surgery can be used in the treatment of these patients instead of the transcatheter aortic valve (AV) replacement (Smith et al. (2011)) when the patient's valves are totally replaced by an artificial valve.

The reconstructed ascending aorta after the aortic root valve-sparing aortic root surgery is shown in Fig. 1. The original valves of the patient are sewed to the inner surface of the graft. The black line running vertically on the outer side of the graft shows the place where the commissures of the valves should be sewed in. These lines are drawn to the grafts during manufacturing and the three lines have even angle distribution on the tube's surface. This currently used common practice assumes that the valves are distributed evenly around the circle defined by the aorta wall. However, patients have their own specific commissure angle distribution (Szymczyk et al.;

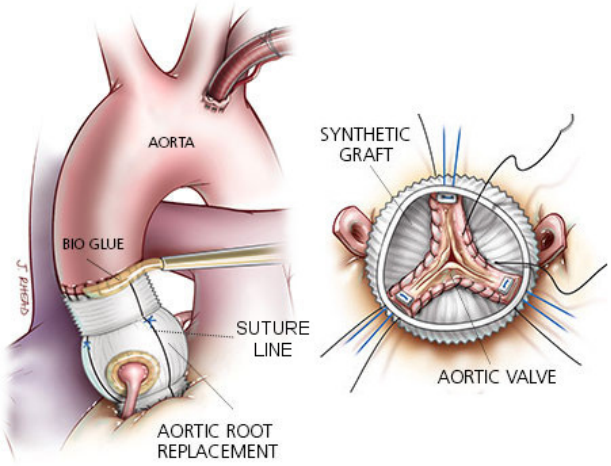

Fig. 1. David procedure, the valve-sparing aortic root surgery [1].

Piazza et al.), which is usually ignored during the surgical intervention and - as it mentioned above - the valves are sewed in the predefined even distribution.

The measurement of patient specific valve angles is not straightforward during the operation which was the main reason for applying uniform even distribution of the valve angles. However, recently special tools have been developed (Fig. 3) that make this measurement accurate and

[1] Image courtesy of Intermountain Medical Center Heart Institute (https://intermountainhealthcare.org/services/heart-care/treatment-and-detection-methods/aortic-root-replacement/)

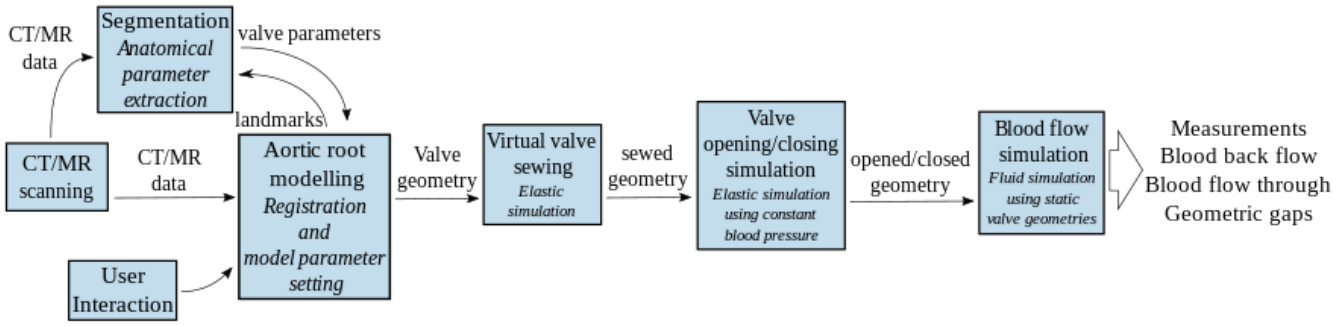

Fig. 2. Overview of the modelling and simulation workflow to compare hemodynamic function of different surgery outcomes(Kacsó et al.).

Fig. 3. Measurement device for the accurate and easy measurement of the angles of valve commissure positions on the aorta wall during the open hart surgery.

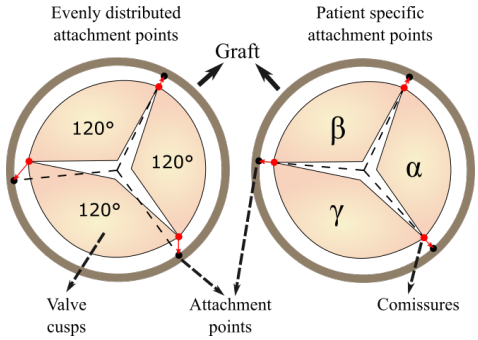

Fig. 4. Valve sewing methods with even and with patient specific leaflet angle distribution (Umenhoffer et al.).

fast (Umenhoffer et al.) and making possible the use of the patient specific distribution of valves during valve replacement. The physiological benefits of this surgery technique allowing more accurate reconstruction of the original physiological setup has not been analyzed yet even though there can be significant differences between the two valve sewing methods as it is shown in Fig. 4.

The aim of the research presented in this paper is the development of modeling and simulation methods for the analysis of alternative versions of the of the valve-sparing root surgery, i.e. sewing the valve leaflets in different angle distribution. The overall goal of the research program is the assessment of hemodynamic functions of the resulted aortic valves. The initial results of the geometric model development allowing the definition of patient specific valve setups have been presented in (Umenhoffer et al.). In that paper a modeling and simulation framework has been introduced to create patient specific geometric models of the aortic root with the valve leaflets. Using the patient specific geometric models the valve opening and closing can be simulated in case of the alternative surgery techniques sewing the valves into different positions. Measuring the blood back flow and flow through the geometric gaps between valve leaflets will provide us the necessary information to estimate the hemodynamic function of the valve after the surgery intervention.

In the subsequent sections – after the brief introduction of the modeling and simulation workflow – the parametric valve model (allowing the patient specific valve geometry definition) is described which will be the input of the surgical intervention simulation. Using the original aortic root geometry and simulating the alternative surgical interventions the result of the interventions can be created. These valve geometries then will be analyzed by simulating the valve movements in response to blood flow. These simulation methods are described in details in this paper accompanied by a parameter study allowing the initial validation of the methods. The output of the simulation methods can be used to asses the important hemodynamic parameters (e.g. back flow of the valve) of the patient similarly to the methods applied in cardiac echocardiography.

2. NUMERICAL SIMULATION METHOD

The main workflow implemented in the modeling and simulation framework is shown in Fig. 2. To create the patient specific aortic root models medical imaging data, particularly high resolution CT or MR scans are used. These images are the input of the modeling procedure and used to define the patient specific valve model, described in Section 2.4. The definition of the patient parameters is partially automated and supported by several segmentation and image processing functions, however it still requires user interaction (see Umenhoffer et al.).

We are interested in the valve functions after surgery so the exact patient specific aortic root model parameters are basically used only to define the parameters of the valve geometry created during the surgery. The valve's leaflet parameters are used directly, the parameters of the anulus are used to define the size of the implanted graft. The grafts has a simple tubular shape which can be modeled analytically in contrast to the more complex shapes of the sinuses of valsava (see Fig. 5).

The back-flow of the blood through the imperfectly closed arterial valves depends on the cross-sectional area of the gap between the leaflets and the pressure difference between the aorta and the left ventricle. The simulation

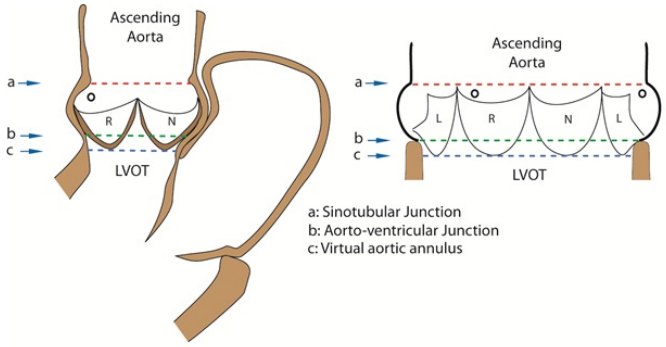

Fig. 5. The anatomy of the aortic root and aortic valves (Daniel et al. (2013)).

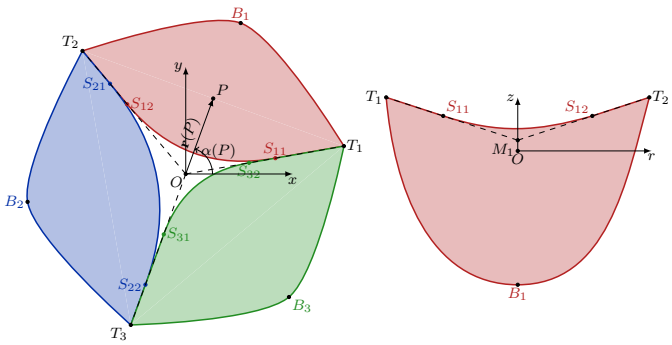

Fig. 6. Tricuspid valve model geometry. On the left, the three valve leaflets are shown in different colors viewed from the direction of the ascending aorta. On the right, one separate leaflet is shown in a side-view. O denotes the center of the cylindrical coordinte system with the polar plane lying in the $x-y$ plane and polar angle is measured from the x axis in the positive direction around the z axis. The commissure points are T_1 T_2 and T_3. The closest points of the leaflets to the Anulus are B_1 B_2 and B_3. Points S_{11}, S_{12}, S_{21}, S_{22}, S_{31}, S_{32} are auxiliary points marking the circular and linear initial representation of the top edge of the leaflets.

method presented in this paper aims the calculation of the former quantity after the surgical intervention. The leaflets block the blood flow where the edges - and the corresponding surfaces - of the leaflets are in contact with each other and allow pathological back-flow (leakage) through the open area. This disease is the so-called aortic valve regurgitation.

With the aim to determine the contact areas of the repaired leaflets upon closure as a function of certain geometric parameters, we adopted a simplified geometry, material model, loading and boundary conditions described in the following subsections.

2.1 Boundary conditions

We simulate solely the three leafets separated from their surroundings. The only kinematic constraints are the prescribed displacements of the leaflet outer edges mapping the original measured curve of intersection of the leaflets and the aorta to the desired target location after the surgery. The static boundary condition is a uniform non-conservative follower pressure ($p = 10$ kPa representing the diastolic pressure difference of 80 Hgmm) applied on the upper surface of each leaflet.

2.2 Material model

To account for large deformations a hyperelastic incompressible neo-Hookean material model is chosen with strain energy density function $W = C_1(I_1 - 3)$, where $C_1 = 5$ MPa (corresponding to half of the shear modulus of the linear elastic material model), and I_1 is the trace of the right Cauchy-Green deformation tensor ($\mathbf{C}$).

2.3 General behaviour

The model incorporates the geometric nonlinearity of large displacements and deformations, the material nonlinearity of the hyperelastic model, and the nonlinearity of the boundary conditions due to the frictionless contact and the non-conservative pressure.

2.4 Geometry

A fully parametric geometry description is created, shown in Fig. 6.

Initial geometry Initial geometry is the original geometry of the patent's aortic root before the surgery. In total, 27 input parameters are needed for the initial geometry: 12 to construct the projection to the $x-y$ plane, further 9 height coordinates, and 6 parameters describing the sag of the leaflets to complete the 3D geometry definition.

The cylindrical coordinates are:

(1) Angles of the commisures:
- $\alpha_{t1} = \alpha(T_1) = \alpha(S_{11}) = \alpha(S_{32})$
- $\alpha_{t2} = \alpha(T_2) = \alpha(S_{21}) = \alpha_(S_{12})$
- $\alpha_{t3} = \alpha(T_3) = \alpha(S_{31}) = \alpha_(S_{22})$

(2) Radii of the leaflet commissures:
- $R_{t1} = r(T_1)$; $R_{t2} = r(T_2)$; $R_{t3} = r(T_3)$

(3) Radii of the leaflet separations (the two sides of the leaflet are chosen to be equal considering the equilibrium of membranes):
- $R_{s1} = r(S_{11}) = r(S_{12})$
- $R_{s2} = r(S_{21}) = r(S_{22})$
- $R_{s3} = r(S_{31}) = r(S_{32})$

(4) Radii of the lowermost points of the leaflets:
- $R_{b1} = r(B_1)$; $R_{b2} = r(B_2)$; $R_{b3} = r(B_3)$

(5) Heights of the leaflet commissures above the $x-y$ plane
- $h_{t1} = h(T_1)$; $h_{t2} = h(T_2)$; $h_{t3} = h(T_3)$

(6) Heights of the lowermost points of the leaflets relative to the $x-y$ plane
- $h_{b1} = h(B_1)$; $h_{b2} = h(B_2)$; $h_{b3} = h(B_3)$

(7) Heights of the fictitious intersection points of the top edges of the leaflets above the $x-y$ plane.
- $h_{m1} = h(M_1)$; $h_{m2} = h(M_2)$; $h_{m3} = h(M_3)$

(8) Elevation angles of the director curves at the lowermost points (β_{b1}, β_{b2}, β_{b3}) and the complementary elevation angles of the director curves at the mit point of the top edge of the leaflet (β_{t1}, β_{t2}, β_{t3}) completing the description of the parabola seving as the descriptor of the sagging property of the final Coons patches describing the leaflets.

Target geometry Target geometry is the aortic root model after the surgery. The target geometry requires further 9 in-plane coordinates and 6 height parameters:

(1) Target angles of the commisures:
- $\tilde{\alpha}_{t1} = \alpha(\tilde{T}_1)$; $\tilde{\alpha}_{t2} = \alpha(\tilde{T}_2)$; $\tilde{\alpha}_{t3} = \alpha(\tilde{T}_3)$

(2) Target radii of the commisures:
- $\tilde{R}_{t1} = \mathbf{r}(\tilde{T}_1)$; $\tilde{R}_{t2} = \mathbf{r}(\tilde{T}_2)$; $\tilde{R}_{t3} = \mathbf{r}(\tilde{T}_3)$

(3) target radii of the lowermost points of the leaflets:
- $\tilde{R}_{b1} = \mathbf{r}(\tilde{B}_1)$; $\tilde{R}_{b2} = \mathbf{r}(\tilde{B}_2)$; $\tilde{R}_{b3} = \mathbf{r}(\tilde{B}_3)$

(4) Target heights of the top of the leaflets above the $x-y$ plane:
- $\tilde{h}_{t1} = h(\tilde{T}_1)$; $\tilde{h}_{t2} = h(\tilde{T}_2)$; $\tilde{h}_{t3} = h(\tilde{T}_3)$

(5) Target heights the lowermost points of the leaflets relative to the $x-y$ plane:
- $\tilde{h}_{b1} = h(\tilde{B}_1)$; $\tilde{h}_{b2} = h(\tilde{B}_2)$; $\tilde{h}_{b3} = h(\tilde{B}_3)$

Tilde indicates the characteristic points of the target geometry.

2.5 Finite Element Modeling

Geometry The geometric model was created via a Python script driving the SpaceClaim modeller, while the simulation of the problem was done by the Mechanical solver in the Workbench environment of the Ansys v19.2 framework. The utilized elements are the SHELL281 quadratic shell element for the leaflet, and the CONTA174 and TARGE170 elements for the surface contact and target effect respectively.

Discretization The mesh convergence study with the sum of the contact surface area as control parameter against the division of the top and bottom curve is depicted by Fig. 7, where the initial and target geometric parameters describing a rotational symmetric geometry are listed in Tables 1 and 2.

Table 1. Parameters of the initial geometry

$\alpha = \alpha_{t1} = \alpha_{t2} = \alpha_{t3}$	120°
$R_t = R_{t1} = R_{t2} = R_{t3}$	15 mm
$R_s = R_{s1} = R_{s2} = R_{s3}$	8 mm
$R_b = R_{b1} = R_{b2} = R_{b3}$	15 mm
$h_t = h_{t1} = h_{t2} = h_{t3}$	5 mm
$h_b = h_{b1} = h_{b2} = h_{b3}$	-10 mm
$h_m = h_{m1} = h_{m2} = h_{m3}$	1 mm
$\beta = \beta_{t1} = \beta_{t2} = \beta_{t3} = \beta_{b1} = \beta_{b2} = \beta_{b3}$	10°

Table 2. Parameters of the target geometry

$\tilde{\alpha} = \tilde{\alpha}_{t1} = \tilde{\alpha}_{t2} = \tilde{\alpha}_{t3}$	120°
$\tilde{R}_t = \tilde{R}_{t1} = \tilde{R}_{t2} = \tilde{R}_{t3}$	13.8 mm
$\tilde{R}_b = \tilde{R}_{b1} = \tilde{R}_{b2} = \tilde{R}_{b3}$	13.8 mm
$\tilde{h}_t = \tilde{h}_{t1} = \tilde{h}_{t2} = \tilde{h}_{t3}$	5 mm
$\tilde{h}_b = \tilde{h}_{b1} = \tilde{h}_{b2} = \tilde{h}_{b3}$	-10 mm

The relative error compared to the target value of the finest discretization (360 element/curve) is less than 7% even for the coarsest division. Based on the mesh convergence curve the edge division number of 180 is selected

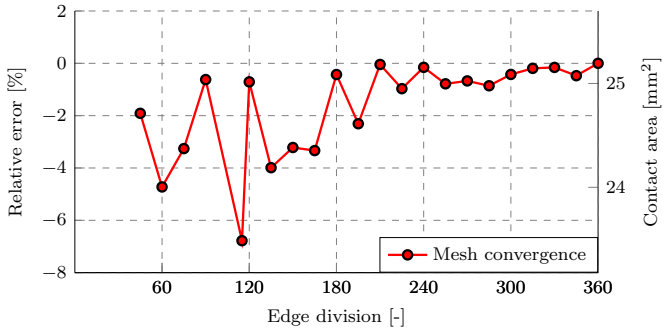

Fig. 7. Mesh convergence study.

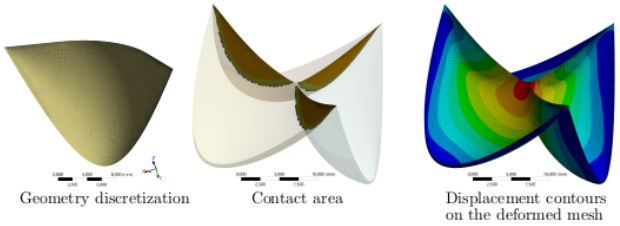

Fig. 8. Test simulation results

as a reasonable compromise between the modeling accuracy and the necessary calculation resources used for the simulation.

A sample geometric discretization, the resulting contact surfaces and the displacement contours of the deformed mesh are shown in Fig. 8.

3. RESULTS

3.1 Parameter Study

We posed the question whether an originally asymmetric dilated geometry ($|\alpha_{t2} - \alpha_{t1}| \neq |\alpha_{t3} - \alpha_{t2}| \neq |\alpha_{t1} - \alpha_{t3}|$) should either be surgically repaired to a target with rotational symmetry in the x-y plane or to a shape congruent to the original projected geometry. To study the question we measured a real leaflet geometry with the following original parameters:

Table 3. Parameters of the measured initial geometry

	$\alpha_{t1} = 0°$ $\alpha_{t2} = 101°$ $\alpha_{t3} = 237°$	
$R_{t1} = 12.1$ mm $R_{t2} = 13.9$ mm $R_{t3} = 11.0$ mm	$R_{s1} = 6.05$ mm $R_{s2} = 6.95$ mm $R_{s3} = 5.50$ mm	$R_{b1} = 12.29$ mm $R_{b2} = 11.77$ mm $R_{b3} = 10.92$ mm
$h_{t1} = 16.86$ mm $h_{t2} = 16.86$ mm $h_{t3} = 16.86$ mm	$h_{m1} = 15.03$ mm $h_{m2} = 15.03$ mm $h_{m3} = 15.03$ mm	$h_{b1} = 0.0$ mm $h_{b2} = 0.0$ mm $h_{b3} = 0.0$ mm
$\beta_{b1} = 10°$ $\beta_{b2} = 10°$ $\beta_{b3} = 10°$	$\beta_{t1} = 10°$ $\beta_{t2} = 10°$ $\beta_{t3} = 10°$	

Here $\tilde{\alpha}_2$ – being the only parameter of the study – ranges from the original 101° via the symmetric 120° up to 139° by 1° steps. All other parameters are fixed. Fig. 9 shows the effect of the asymmetry of the target geometry on the

Table 4. Prescribed repair parameters

$\tilde{\alpha}_{t1} = 0°$		
$\tilde{\alpha}_{t2}$: from 101° to 139° by 1°		
$\tilde{\alpha}_{t3} = 240°$		
$\tilde{R}_{t1} = 11.44$ mm	$\tilde{R}_{b1} = 12.29$ mm	
$\tilde{R}_{t2} = 13.15$ mm	$\tilde{R}_{b2} = 11.77$ mm	
$\tilde{R}_{t3} = 10.40$ mm	$\tilde{R}_{b3} = 10.92$ mm	
$\tilde{h}_{t1} = 16.86$ mm	$\tilde{h}_{b1} = 0.0$ mm	
$\tilde{h}_{t2} = 16.86$ mm	$\tilde{h}_{b2} = 0.0$ mm	
$\tilde{h}_{t3} = 16.86$ mm	$\tilde{h}_{b3} = 0.0$ mm	

three contact areas, while Fig. 10 shows the loaded shapes of various target geometries.

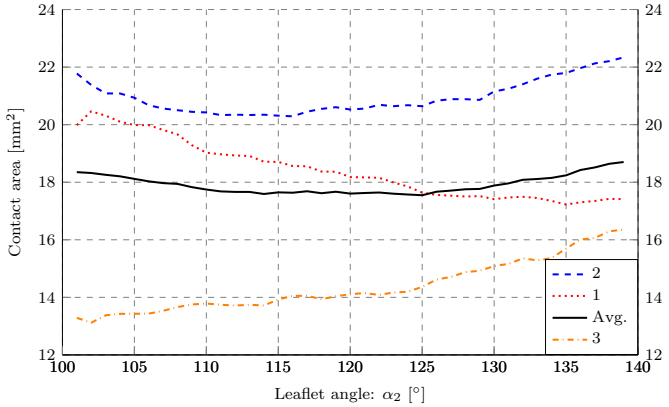

Fig. 9. Effect of the target commissure angles on the contact area of the valve leaflets. The angle of the second commissure is changed from 101° to 139° and the contact area of the leaflets are calculated and shown on the vertical axes. All the three leaflet pairs are examined (the three colored dashed lines with numbers indicting the corresponding commisures), the average contact area is shown by the black solide line.

3.2 Simulation Results

In our example the largest contact area ($\tilde{a}_2$) is the one involving the smallest and the largest opening angles, the smallest contact area ($\tilde{a}_3$) is the one between the middle and the largest opening angles. This relation does not alter with the target angle in our regime, although the smallest ($\tilde{a}_3$) approaches the intermediate one ($\tilde{a}_1$) with increasing $\tilde{\alpha}_2$. Regarding our original question of the effect of asymmetry, we can only conclude here, that the average, and thus the sum of the contact areas show a slight change and approach their undesired minimum at the symmetric case ($\tilde{\alpha}_2 = 120°$) suggesting a better yet not optimal target geometry similar to the original. Trivially, the monotonously increasing contact area, $\tilde{a}_3$ is surrounded by the unchanged opening angle ($\Delta\tilde{\alpha}_{13}$) and the decreasing one ($\Delta\tilde{\alpha}_{32}$), while the monotonously decreasing contact area, $\tilde{a}_1$ is surrounded by the unchanged opening angle ($\Delta\tilde{\alpha}_{13}$) and the increasing one ($\Delta\tilde{\alpha}_{21}$). We propose, that the continuous increase in the minimal contact area, which is a good measure of the quality of the repair, in our particular case is caused by leaflet 2 being extremely stretched out compared to the other two even in the unloaded geometry. This is to be further analyzed in the future.

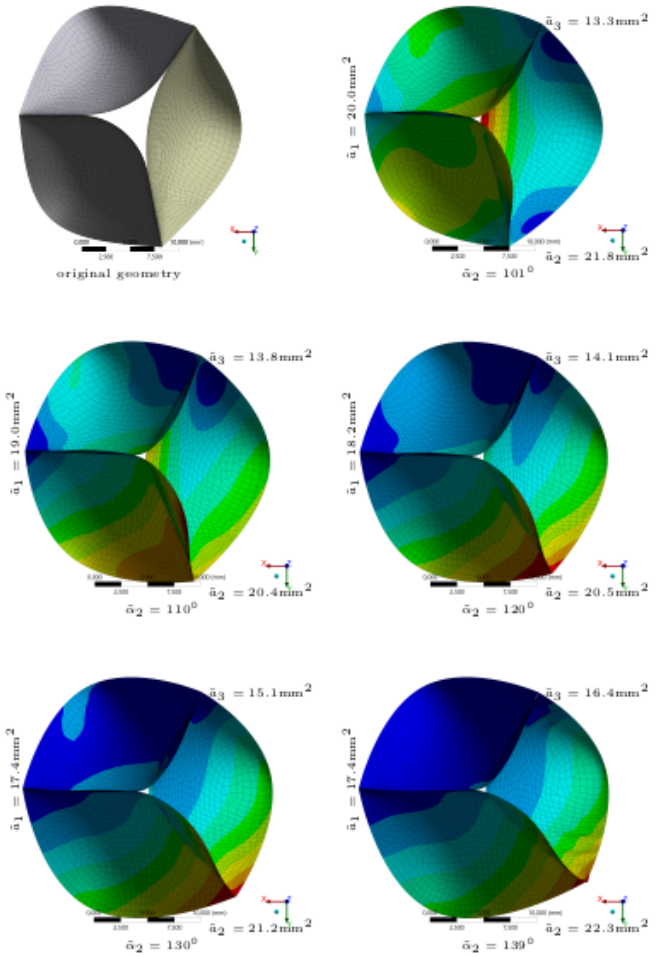

Fig. 10. Loaded shapes – showing the closed valve leaflets – of various target geometries. The model of the original configuration of the valve leaflets are shown in the top left corner. Five other simulated models are shown with different commissure angle distributions, the actual angles are shown under the figures together with the contact areas at the corresponding locations. The color code represents the distance between the original and final position of the leaflet surface elements, thus being solely a simulation artifact.

4. DISCUSSION

A finite element simulation method of the aortic valve leaflets is presented that can be used to analize leaflet setups after surgical interventions. Optimal simulation paramerst were identified in a mesh convergence study (Fig. 7).

The parameters of the geometric leaflet model used in this study were defined based on a CT scan of a real adult patient with an average size hart (Umenhoffer et al.).

In the parameter study alternative surgical interventions were compared. The first important outcome of the study is the initial validation of the proposed simulation method. As the angle of the leaflet was adjusted between 101° and 139° 39 different surgical interventions were simulated. All of these simulated outcomes are found to be physiologically viable - several of these were shown in Fig. 10 - and

credible. This confirms the applicability of the method for the analysis of the aortic valve geometries.

This validation is just an initial step of a larger scale analysis where aortic roots from different size harts will be modeled and analyzed in the presented way. Since the accurate visualization of the aortic valve leaflet motion is challenging in its physiological environment only the imaging techniques providing still images can be used for the comparison of the simulation results and the real valves function. 33 aortic valves are already segmented by the introduced modeling framework in order to provide sufficient size data base for validation.

In the study the contact area of the valve leaflets is defined as a quantitative measure of the robustness of the aortic valve closing. From the biomechanical aspect this is definitely a proper parameter for describing the robustness of the valve closing function. However, the limitations of this parameter for the description of the medical aspects should be analysed in the future.

The main outcome of the simulation study from the aspect of the overall goal of this research, however, the results shown in Fig. 9. The average contact area shown by the solid black line has its minimum around 120°. 120° represents the valve leaflet position that would be selected according to the current common surgical practice when the even distribution of the valve angles if forced. According to this simulation study all other options would have been resulted in larger average contact area of the valve leaflets, thus more robust valve function. Even though it is just a single case where the use of the original leaflet angles would probably result in better outcome of the cardiac surgery but it is a real example simulated by using a patient specific aortic root model of a real data. This result definitely outlines the importance and medical impact of this study.

4.1 Modeling Results and Limitations

We presented an easy-to-use simplified model of the tricuspid valve requiring minimal user interaction. It serves as an efficient tool to investigate the effect of geometric properties on several physiologically important geometric and biomechanical parameters from which we presented an introductory example. The limitations of the model are its lack of the surrounding tissues and fluid–solid interaction, the static loading nature, and the pure hyperelastic material model. All of which are to be addressed in our further studies of more complex geometry involving the aortic stem, the pulsatile load of the blood flow and an improved visco-plastic material model. Note, that the elastic behaviour causes limitations on the achievable target geometry even in this simple case by the possibility of unrealistic buckling shapes at certain compressed parts, as was the case for leaflet 2 when $\tilde{\alpha}_2 > 139°$. This limit can be further increased even in the implicit simulation with a plastic material model in the compressive regime.

5. CONCLUSION

A modeling environment and a finite element simulation method is presented for the analysis of the variations of the valve-sparing aortic root surgery intervention. The simulation method is validated by a parameter study using the patient specific aortic root model of a real patient. The initial results suggest that the currently used surgical practice can be improved and repairing the original, asymmetric geometry of the aortic leaflets may result in better cardiac parameters.

ACKNOWLEDGEMENTS

The research was supported by the Hungarian National Scientific Research Foundation, Grant No. K116574, by the BME-Biotechnology FIKP grant of EMMI (BME FIKP-BIO), and by the EFOP-3.6.1-16-2016- 00017.

REFERENCES

Daniel, Z., Michael, K., and Ernesto E., S. (2013). A Framework for the Systematic Characterization of the Aortic Valve Complex by Real-Time Three Dimensional Echocardiography: Implications for Transcatheter Aortic Valve Replacement. In A. Squeri (ed.), *Hot Topics in Echocardiography*. InTech.

David, T.E. (2010). Surgical treatment of ascending aorta and aortic root aneurysms. *Progress in cardiovascular diseases*, 52(5), 438–444.

Kacsó, Á., Szécsi, L., Tóth, M., Benyó, B., and Umenhoffer, T. (2018). Finite volume blood flow simulation for highly deformable boundaries.

Piazza, N., de Jaegere, P., Schultz, C., Becker, A.E., Serruys, P.W., and Anderson, R.H. (2008). Anatomy of the Aortic Valvar Complex and Its Implications for Transcatheter Implantation of the Aortic Valve, . *Circulation: Cardiovascular Interventions*, (1), 74–81. doi:10.1161/CIRCINTERVENTIONS.108.780858.

Smith, C.R., Leon, M.B., Mack, M.J., Miller, D.C., Moses, J.W., Svensson, L.G., Tuzcu, E.M., Webb, J.G., Fontana, G.P., Makkar, R.R., et al. (2011). Transcatheter versus surgical aortic-valve replacement in high-risk patients. *New England Journal of Medicine*, 364(23), 2187–2198.

Szymczyk, K., Polguj, M., Szymczyk, E., Bakoń, L., Pacho, R., and Stefańczyk, L. (2016). Assessment of aortic valve in regard to its anatomical variants morphology in 2053 patients using 64-slice CT retrospective coronary angiography . *BMC Cardiovascular Disorders*, (1), 89.

Teo, E.P. and Isselbacher, E.M. (2019). In *Essential Echocardiography", Diseases of the Aorta* .

Umenhoffer, T., Tóth, M., Kacsó, Á., Szécsi, L., Szlávecz, Á., Somogyi, P., Szilágyi, L., Kubovje, A., Szerafin, T., Szirmay-Kalos, L., and Benyó, B. (2018). Modeling and simulation framework of aortic valve for hemodynamic evaluation of aortic root replacement surgery outcomes". *IFAC-PapersOnLine*, (27), 258–263. doi: 10.1016/j.ifacol.2018.11.632. 10th IFAC Symposium on Biological and Medical Systems BMS 2018.